TUDelft

Delft University of Technology

Metal-insulator multilayer precursors for enhanced Sm^{2+} absorption and Tm^{2+} luminescence in SiAlO thin films prepared by magnetron sputtering

Bosco, G. B.F.; van den Biesen, J. K.; Boers, C. D.; Simone, G.; Kao, J.; Tichelaar, F. D.; Boshuizen, B.; van der Kolk, E.

Important note
To cite this publication, please use the final published version (if applicable).
Please check the document version above.

Metal-insulator multilayer precursors for enhanced Sm^{2+} absorption and Tm^{2+} luminescence in SiAlO thin films prepared by magnetron sputtering

G.B.F. Bosco [a,*,1], J.K. van den Biesen [a], C.D. Boers [a], G. Simone [b], J. Kao [b], F.D. Tichelaar [c], B. Boshuizen [d], E. van der Kolk [a,**]

[a] *Luminescence Materials, Delft University of Technology, Mekelweg 15, 2629, JB, Delft, the Netherlands*
[b] *Physee BV, Van Mourik Broekmanweg 4, 2628, XE, Delft, the Netherlands*
[c] *Kavli Institute of Technology, Quantum Nanoscience, Delft University of Technology, Delft, the Netherlands*
[d] *Department of Chemical Engineering, Delft University of Technology, 2629, HZ, Delft, the Netherlands*

ARTICLE INFO

ABSTRACT

Silicon-aluminum-oxigen (SiAlO) coatings doped with Sm^{2+} and prepared by reactive magnetron co-sputtering of Si, Al, and Sm targets, are attractive for luminescence solar concentrator applications but suffer from the low absorption between 300 and 600 nm. This article reports that the main cause of low absorption is a high concentration of undesired Sm^{3+}. This finding is supported by optical transmittance, photoluminescence emission and excitation characterization, and X-ray photoelectron spectroscopy data of the Sm's $3d^{5/2}$ edge. We present an alternative deposition process for obtaining Sm doped SiAlO layers with enhanced Sm^{2+} absorption by incorporating Sm through the use of multilayer thin-film precursors composed of metallic Sm and SiAlO layers. After thermal post-deposition treatments, diffusion and reaction of the metallic Sm layers with the SiAlO host results in coatings showing the characteristic $5d \rightarrow 4f$ transitions of Sm^{2+} in the region between 250 and 600 nm which were not detectable in Sm-doped single layers. This same deposition strategy produces Tm doped SiAlO coatings with Tm^{2+}'s characteristic luminescence at 1132 nm when the SiAlO host is in the mullite composition region. The photoluminescence excitation spectrum of Tm^{2+} is compared to phosphor with similar composition and covers the range between 300 and 700 nm.

1. Introduction

Luminescent Solar Concentrators (LSCs) have strong potential to be part of future net-zero-energy buildings if applied as electricity-generating windows [1]. As a sputter-coated thin film doped with luminescent centers on glass, LSCs absorb part of the solar spectrum and, because of total internal reflection in the film and glass' interface, downshift the incoming light towards the edges of the glass where photovoltaic cells convert this concentrated light to electricity. In an efficient solar concentration process, the thin film ideally absorbs 30% of the spectral range from 350 to 900 nm and emits without self-absorption over a narrow wavelength range that can be converted efficiently by Si, CIGS, or CIS solar cells [2].

Silicon-aluminum-oxygen-nitrogen (SiAlON) coatings are widely used in the glass industry for anti-reflection and scratch protection purposes and have the additional advantage of not scattering any sunlight.

Previously, it was shown that Eu luminescence can be used to further functionalize these materials as LSCs [3]. However, the 5d-states of Eu^{2+} have a limited absorption spectral range and its emission suffers from self-absorption. More recently, divalent samarium (Sm^{2+}) has demonstrated its potential as LSC active ion in SiAlO coatings [4,5]. Sm^{2+} luminescence can be excited in the visible range by $4f^{5}5d^{1} \rightarrow 4f^{6}$ transitions. Besides, the $4f^{6} \rightarrow 4f^{6}$ emission transitions of Sm^{2+} do not suffer from self-absorption due to inter-configurational and non-radiative relaxation via $4f^{5}5d^{1} \rightarrow 4f^{6}$ transitions (see Fig. 1**A**). This results in a

wider absorption range up to 600 nm in the visible spectrum. Although high luminescent intensity was observed, Sm^{2+}-related absorption remained surprisingly low [5]. The absorption spectra showed absorption intensity of the order of 1%, or even lower at specific wavelengths, despite relatively thick (3–4 μm) and highly Sm-doped (2–8 at.%) films. It contrasts with the work on Eu^{2+} doped SiAlON thin films [6]. Sputtered under similar conditions, the absorption reported from the $4f^6 \rightarrow 4f^55d^1$ transitions of Eu^{2+}, was 30–50% in 400–600 nm thick gradient thin films with about 10 at.% of Eu^{2+} doping. One hypothesis raised to explain the low Sm^{2+} absorption was that, when Sm was inserted in sputtered SiAlO coatings, metallic Sm or Sm_2O_3 nano-inclusion could be present. Another hypothesis was that both the desired Sm^{2+} valence state but also the trivalent (Sm^{3+}) oxidation state were present. In this work, we show that the main cause for the reported low absorption of Sm^{2+} in Sm doped SiAlO (SiAlO:Sm), in contrast to Eu^{2+}, is that Sm is present as Sm^{3+}.

Sm^{3+} is not desirable because the orange photoluminescence of Sm can be excited in the visible only through much weaker $4f^6 \rightarrow 4f^6$ transitions. The more intense charge transfer (CT) band of Sm^{3+} is limited typically to the ultraviolet part of the solar spectrum [7,8]. Thus, even with high Sm doping concentrations, thin-film absorption related to Sm transitions can barely be perceived.

One possible way to circumvent the low Sm^{2+} concentration in inorganic materials, at least through single crystal synthesis, is by making use of stronger reducing conditions as in the metal comproportionation reaction (MCR) with metallic lanthanide precursors [9–12]. In MCR, the precursor of the lanthanide element is introduced in the metallic state so it can reduce other lanthanide elements in the material through an equation of the type below:

$$Ln + 2Ln^{3+} \rightarrow 3Ln^{2+} \qquad (1)$$

For us, MCR served as an inspiration for the use of multilayered thin-film precursors (MTFP) composed of SiAlO and metallic layers of Sm (SiAlO/m-Sm) or Tm as precursors of SiAlO:Sm or SiAlO:Tm films with the purpose of producing new coatings with enhanced Sm^{2+} concentration or Tm^{2+} emission. This method is based on the deposition of alternating layers of SiAlO and metallic lanthanoid element. Fig. 1B gives a general schematic representation of one MTFP. SiAlO layers are deposited alternately over metallic lanthanide (m-Ln) layers through several iterations. By alternating the reactive magnetron sputtering of Si and Al targets with non-reactive sputtering of Ln, one SiAlO layer is deposited over one metallic layer. Under subsequent thermal treatment of SiAlO/m-Ln under reducing atmospheres, not only it is possible to increase Sm^{2+} concentration, but also to obtain Tm^{2+} in a material grown in similar conditions than those used for the Sm-doped coatings.

We prove it by showing the photoluminescence characteristics of Tm^{2+}, an ion that is known to be even more difficult to be reduced to the 2+ valence state, and by showing the photoluminescence excitation and emission characteristics of Tm^{2+} in the near-infrared spectrum.

This article is structured as follows: after a description of the experimental methods used in the sample fabrication and characterization, the photoluminescence properties of Sm^{2+} and Sm^{3+} in reactive co-sputtered single layer SiAlO:Sm will be reviewed. X-ray Photoelectron Spectroscopy data (XPS) will be given so the relative concentration of Sm^{2+} and Sm^{3+} can be determined. Next, the method used to prepare MTFP will be presented followed by the enhanced Sm^{2+} absorption. Next, we show that by using MTFP and high temperature rapid thermal annealing Tm^{2+} photoluminescence can be observed. Finally, a conclusion with perspectives on its applicability in glass-industry-compatible LSCs is given.

2. Experimental methods

2.1. Synthesis

The films were grown in an AJA ATC Orion 5 magnetron sputtering system which can accommodate up to four different sputtering targets. The deposition was carried out with a combination of Sm (or Tm), Al, and Si targets with a 5.08 cm diameter each from Demaco. The Sm and Tm targets were of 99.99% purity whereas Si and Al were 99.9%. The Al target is powered by a direct current supply whereas the other two guns are powered by two radio frequency alternating supplies. With the base pressure being typically below 10^{-6} Torr, the sputtering of all the layers was performed at a working pressure of 3.0 mTorr. The pressure is sustained by different combinations of 5 N purity Ar and O_2 gas flows. For sputtering of the metallic RE layers, the pressure is sustained by a gas flow of 5 N purity Ar and for reactive sputtering by a mixture of Ar and 5 N O_2. The thin-films were either deposited at room temperature (RT) or at 200 °C. The specific deposition conditions used for growing each sample are summarized in Tables 1 and 2. To identify each sample while discriminating the synthesis method used for each we have opted for adding a prefix to the sample name: "SL" indicates the films grown using the conventional single-layered coatings by reactive magnetron co-sputtering; "ML" indicates the films prepared by using MTFP - method described in this work; and "SG" the phosphors prepared by sol-gel sintering. For example, "SLSm1″" indicates a unique single-layered SiAlO:Sm thin-film and "MLTm1" indicates a unique MTFP grown with metallic Tm interlayers.

Prior to each thin-film deposition, substrates are prepared through a substrate biased sputtering procedure with the chamber filled with pure
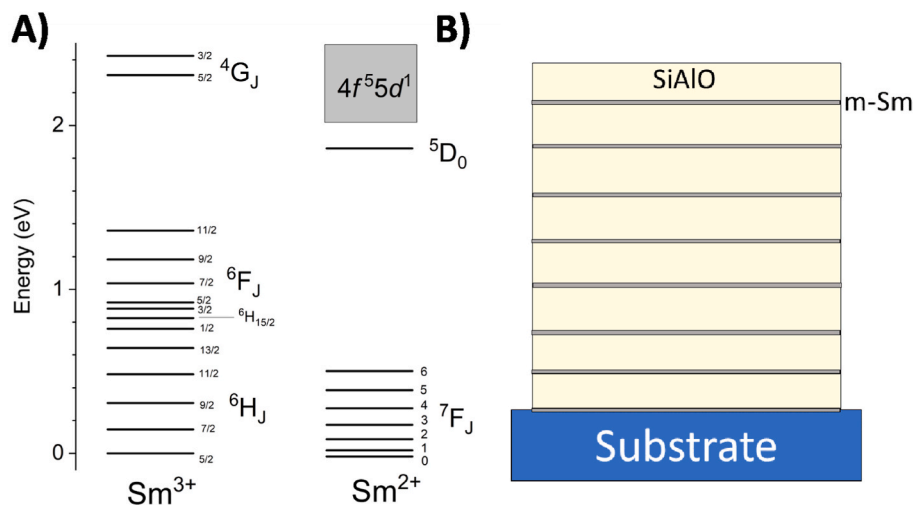
Fig. 1. A) Schematic energy level diagram of both Sm^{3+} (left) and Sm^{2+} (right) associated with the transitions in the visible range of the spectrum. The lines represent $4f^6$ states whereas the rectangle represents a combination of broad $4f^55d^1$ states. Energy values from Ref. [13]; B) Schematic representation of one multilayered thin-film structure. The structure is composed of Ln layers, sputtered using metallic conditions on the m-Ln target, interspersed with SiAlO layers, reactively sputtered using fully oxidized Si and Al targets.

Table 1
Conditions used in reactive magnetron co-sputtering of Si, Al, and Sm targets for the deposition of single-layered SiAlO:Sm thin-films.

Sample ID	Dur. (s)	Subst. T. (°C)	Anneal. T. (°C)	Si/Al (W)	Si (W)	Sm (W)	Al (W)	Ar (sccm)	O₂ (sccm)
SLSm1	27,000	200	575	N/A	130	30	20	18	1.2
SLSm2	40,500	RT	400	N/A	130	25	20	18.4	1.2
SLSm3	27,000	RT	1200	N/A	130	35	20	18	1.0
SLSm4	12,500	RT	1200	N/A	50	30	65	30.5	1.5
SLSm6	10,000	RT	650	120	N/A	15	N/A	14.1	0.9

The conditions considered here are: deposition duration, substrate temperature, annealing temperature, gas flows, and fixed powers used for each target. RT indicates room temperature.

Table 2
Process parameters used for deposition of MFTS. One SiAlO layer is grown after one lanthanide metallic layer and their deposition duration are indicated in sequence; e.g., 215/2500 indicates that the deposition duration of the metallic layer was 215 s. This was followed by the growth of one SiAlO layer for 2500 s. The multi-step rapid thermal annealing procedure is characterized by two temperatures, each describing one annealing step and their corresponding duration. For the SiAlO layers, Ar and O₂ flows were respectively 30.5 and 1.5 sccm (conditions that fully oxidized both Si and Al targets). For the deposition of metallic Ln (m-Ln) layers, the oxygen flow was set to zero and Ar to 32 sccm. All samples were prepared with the substrate at room temperature. Except for MLTm2, fabricated over a c-Si substrate, all other films are fabricated over UV-fuse silica glass substrates.

Sample ID	Dur. (s)	Anneal. T (°C)	Anneal. Dur. (s)	Si (W)	m-Ln (W)	Al (W)	No.
MLSm1	215/2500	400/1200	1800/20	50	20	65	14
MLSm2	275/2450	400/1200	1800/20	50	30	65	16
MLTm1	125/2500	250/1200	1800/20	50	30	65	14
MLTm2	215/2500	N/A	N/A	50	30	75	14

Ar (32 sccm) for 5 min at a fixed power of 20 W. The substrate holder is centrally situated 17.8 cm apart of all four targets. The substrate holder was either rotated at a constant speed of 30 rpm to ensure a laterally homogeneously sputtered sample or was deliberately kept still for fabricating films with gradient composition and thickness (films of Table 1). Further details about the used magnetron sputtering system can be found in Refs. [3,5].

2.2. X-ray photo-electron spectroscopy (XPS)

The XPS spectra were obtained using a ThermoFisher K-alpha XPS system equipped with a monochromatic Al anode X-ray source radiating at 1484 eV to excite the sample with an actual spot size of 400×770 μm². The cathode was set to 12 kV and the beam current to 3 mA. The photo-electrons are detected by a 128-channel detector, with a 0.1 eV resolution. During data collection, a dual source flood gun was used at 1 V and 100 μA to mitigate sample charging. Ion etching was used when the sample had to be cleared from surface adventitious carbon. In both cases the surface material, over a 4×2 mm² area, was removed through mono-atomic argon sputtering with the ion gun voltage set at 200 V. The spectra were recorded at an operating pressure of approximately 0.4 μTorr. For survey spectra, the pass energy and step size were set to 200 eV and 1 eV respectively, whereas for Sm 3d, Al 2p, Si 2p, O 1s, and C 1s high-resolution spectra were obtained with 50 eV pass energy and 0.1 eV resolution. The spectra were corrected for the non-monochromatic nature of the X-ray source and also for the kinetic energy-dependent transmission of the spectrometer by multiplying each spectral intensity with its corresponding kinetic energy. All spectra were calibrated by assigning the true energy value (284.8 eV) [14] corresponding to the position of a C 1s peak.

Further processing was done in CasaXPS software (version 2.3.22PR1.0) [15]. Convoluted Gaussian–Lorentzian profiles were used for all components of the XPS spectra. A standard Tougaard U3 algorithm was used for background subtraction on all spectra. The local atomic concentration composition of the gradient film was determined by:

$$C_i = \frac{A_i / S_i}{\sum_j A_i / S_i} \qquad (2)$$

where C_i is the atomic concentration of element i, A_i is the peak area, and S_j is the relative sensitivity factor of element j. The library of experimental relative sensitivity factors (R.S·F.) used is an adjusted Scofield library for aluminum sources, specific for the instrument used. The R.S.F. values used were: 1.00 for C 1s, 2.881 for O 1s, 0.90 for Si 2p, 0.56 for Al 2p, and 76.737 for Sm 3d. Due to the spin-orbit interaction there will be coupling between the orbital angular momentum quantum number ($l = 2$) and the spin quantum number ($s = \pm 1/2$). The peak corresponding to the $3d_{3/2}$ level has a lower signal-to-noise ratio than the $3d_{5/2}$ level so only the latter was considered in the quantification of Sm^{2+} vs. Sm.

2.3. Optical characterization

Transmission measurements in the UV-VIS region were conducted by placing the film on top of an integrating sphere and illuminating it with a collimated, 2.7 mm wide spherical beam. In this way, both direct and diffuse transmission are available. Thus, haze can be characterized. In this study, only total transmission is considered. The light source is an Avalight-DH-S deuterium halogen lamp. The incoming and transmitted light is guided through multimode optical fibers to Ocean Optics spectrometer (QE Pro). Automated XY positioning of the sample stage allowed for characterizing the position-dependent transmission over the whole sample surface. More details on the positioning technique and the experiment setup are provided at [3,16].

The software used for fitting single-layered films' transmission was OPTIFIT [17]. This software uses optical parameters based on the work by Swanepoel [18] and the relation between thickness and refractive index from the work of Poelman and Smet [17,19]. The analysis of the UV-VIS transmittance of MTFP was done on RefFIT [20]. The software uses a universal approach, Kramers-Kronig compatible, to model the real and imaginary parts of the dielectric function.

For thickness estimation of MTFP, the advantage of analyzing optical spectra (transmittance, reflectance, etc.), compared to the use of quartz crystal microbalance (QCM) devices, is the possibility of determining the effective thickness with metallic character. This is more evident for Sm and Tm MTFP where the thickness of the layer with metallic character is relevant for determining the film's intended optical properties. Due to the nature of the sputtering process, the incoming neutrals that eventually grow to make a layer can diffuse to form interfaces of about a few nanometers [21–23] and, thereby, react with available oxygen atoms of neighboring layers (or from the substrate itself). In other words, the sputtered ions reach the film with sufficient energy so they can penetrate it and make an interface composed of a mixture with an oxide material. These oxidized layers are usually transparent and do not offer neutral lanthanide atoms that may eventually end up in the less common, but

desired divalent oxidation state.

Another limitation of QCM devices for estimating the thickness of metallic layers in MTFP is the fact that there is a lack of Z-ratio values - used as input for correcting the acoustic impedance difference of the quartz resonator with the desired material. However, the method based on optical transmittance lacks consistent information on the dielectric function of the lanthanide metals in the optical region. This is why we used a method based on optical transmittance and data analysis through RefFIT [20] for estimating the individual layer thicknesses of MTFP. Further details on this method are described in supplementary information.

For the excitation and emission photoluminescence studies, a 450 W xenon lamp was used as the excitation source. The monochromatic excitation was tuned by a Gemini 180 dual grating monochromator in 1 nm steps. Both the excitation light as well as the luminescence were fed through longpass filters for the removal of second order diffraction. The transmitted 685 nm and 1130 nm emission intensity, for Sm^{2+} and Tm^{2+} respectively, was plotted versus the excitation wavelength. The stage was aligned to the sample's surface at 45° with respect to the excitation source. A Hamamatsu R76000U-03, operated at −600 V, was used For the measurements in the VIS. In the NIR, a Hamamatsu H10330A-75 PMT, operated at −900 V, was used instead.

One 6-inch Spectraflect Integrating Sphere was used for quantum efficiency measurements. The sphere's inner surface and attachments are coated in barium sulfate, ensuring high reflectivity. One of the integrating sphere's entrances features a baffle that diffuses the incoming LED light to indirectly excite a sample placed on a coated holder positioned in the center of the sphere. The light output is guided through optical fibers and detected by a QE65000 Ocean Optics CCD spectrometer through a separate exit. Photoluminescence quantum efficiency (η_{PLQE} [%]), as defined in this work, is the ratio between the number of emitted photons over the absorbed photons considering sample indirect excitation and reference spectra obtained with an empty sphere. The number of emitted photons was obtained by integrating the spectral difference between indirect sample illumination and the empty sphere, in the range above 674 nm. The number of absorbed photons was obtained by the difference in the same spectrum in the wavelength range below 674 nm.

2.4. Electron microscopy

The measurements were performed with a FEI cubed Cs corrected Titan. The bright field (BF) images were collected with an objective aperture, to block diffracted electron beams and form an image of transmitted electrons. Annular Dark Field (ADF) images were collected in scanning mode (STEM) using a ≈0.3 nm electron beam. The diffracted electrons were collected on a ring shape detector. The number of diffracted electrons scales with the heavier (larger Z) and thicker part of the sample. Therefore these showed up bright in ADF images. EDX spectra were obtained for each beam position in STEM imaging, using the ChemiSTEM detector from Thermo Fisher. The sample preparation starts with attaching the thin film sample on a Si wafer partly for protection. Subsequently, a cross-section slide is cut and thinned down to ~30 μm. The slice was placed on a copper ring to be thinned down in a Gatan argon mill, allowing for electron transmission. The electron transparent cross-section (foil) forms the region to be investigated. It has a thickness of approximately 150 nm, but increases slightly from the top to the bottom of the film.

A JEOL IT-100 operated at 15 keV was used for SEM/EDS analysis. The energy of the electron beam was chosen to prevent beam penetration and subsequent characteristic X-ray emission from the quartz substrate. Quantitative elemental analysis without a conductive coating was achieved by employing the device in low vacuum mode (35 Pa pressure). Elemental compositions were quantified at $1000 \times$ magnification.

3. Results and discussion

3.1. Divalent Sm concentration in co-sputtered Sm doped SiAlO layers

Sm^{2+} luminescence can be excited by efficient $4f^6 \rightarrow 4f^55d^1$ transitions in the 250–600 nm spectral range. However, as reported earlier [5], in thin-films prepared by reactive magnetron co-sputtering of the Al, Si, and Sm targets, the observed absorption in this spectral range was estimated to be only of the order of 1% despite considering thick (3–4 μm) heavily Sm-doped (2–8 at.%) samples. The possible presence of metallic Sm or Sm_2O_3 agglomerates was one of the hypotheses raised to explain the low Sm^{2+} absorption. Another hypothesis was that both the desired Sm^{2+} valence state, and the undesired Sm^{3+} were present.

The first piece of evidence attesting for a possible high amount of Sm^{3+} in these films comes from photoluminescence emission (PL) and excitation (PLE) studies of two Sm-doped SiAlON samples. One is a powdered phosphor specifically prepared by sol-gel synthesis to exhibit only Sm^{3+} luminescence (SGSm) whereas the other is a single-layered film prepared in very similar conditions as was reported in Ref. [5]. The conditions used to prepare SGSm are summarized in Table 3 and the conditions used during the deposition of SLSm3 are in Table 1.

Fig. 2**A** shows normalized PL and PLE spectra of SGSm. This phosphor has an Al/Si atomic ratio different from what is observed in our films, and, in particular SLSm3, but gives a strong PL signal related to Sm^{3+} when compared to the thin film. The characterization of the PLE of SGSm makes it possible to identify the PLE spectrum related to Sm^{3+} in the region between 300 and 550 nm by monitoring the PL at 649 nm. The observed Sm^{3+} transitions are assigned to intra-configurational $4f \rightarrow 4f$ electronic transitions departing from the common ground state $^6H_{5/2}$. The peaks at 362, 372, and 404 nm, are assigned, respectively, to transitions to $^4H_{7/2}$, $^6P_{7/2}$, and $^4F_{7/2}$ [24]. Considering the range below 250 nm, the PLE spectrum of SGSm shows one absorption peak centered at 220 nm (or 5.64 eV) that is assigned to Sm^{3+} charge transfer band. Considering the range between 550 and 680 nm, the PL is characterized by three peaks. They are assigned to the following Sm^{3+} intra-4f transitions: $^4G_{5/2} \rightarrow {}^6H_{5/2}$ at 566 nm, $^4G_{5/2} \rightarrow {}^6H_{7/2}$ at 600 nm, and $^4G_{5/2} \rightarrow {}^6H_{9/2}$ with peak emission at 648 nm.

Fig. 2**B** shows normalized PL and PLE spectra of SLSm3. The excitation and emission of SLSm3 are characteristic of both Sm^{3+} and Sm^{2+}. This sample shows the same Sm^3 emission lines as observed from the phosphor SGSm in the spectral region between 550 and 650 nm. In the spectral region between 680 and 750 nm, however, three emission lines are related to Sm^{2+}. The responsible transitions are $^5D_0 \rightarrow {}^7F_0$ at 683 nm, $^5D_0 \rightarrow {}^7F_1$ at 700 nm, and $^5D_0 \rightarrow {}^7F_2$ at 726 nm. The PLE spectrum was acquired by monitoring the $^5D_0 \rightarrow {}^7F_0$ transition at 684 nm. The Sm^{2+} transitions between 300 and 550 nm come from transitions of the inter-configurational $4f \rightarrow 5d$ with the most intense peak centered about 360 nm.

Typically, Sm^{3+} $4f \rightarrow 4f$ transitions are of the order of 100 times weaker than the $4f \rightarrow 5d$ transitions of Sm^{2+}. By assuming there is a high concentration of Sm^{3+}, the weak absorption, earlier observed in reactively magnetron co-sputtering single-layer films, can be explained. After all, the Sm concentration in SLSm3 was of the order 2–8 at.%.

Table 3

Preparation conditions of the powdered samples. The composition of SGSm is $Si_{48}Al_2O_{99}$ and it has an amorphous structure. Sample SSRTm has composition $SiAl_4O_8$ and it has an α-alumina and mullite combined crystal structures.

ID	method	$\dfrac{Ln}{(Si+Al)}$ (%)	$\dfrac{Si}{Al}$ (%)	Sint. Temp. (°C)	Duration (h)	Gas
SGSm	sol-gel	1	24	1100	3	N_2/H_2
SSRTm	solid state reaction	0.4	0.25	1500	3	N_2/H_2
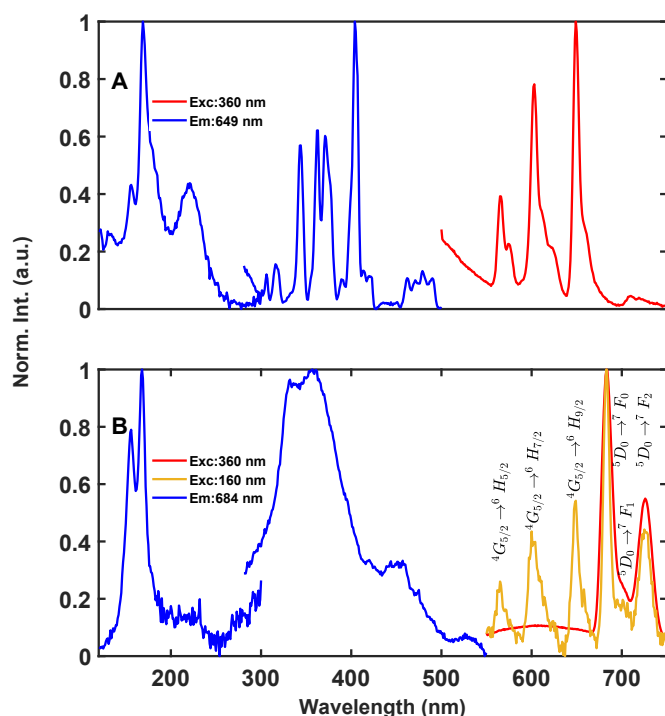
Fig. 2. PL and PLE spectra for phosphor **A)** SGSm and **B)** SLSm3, both recorded at T = 10 K. All spectra are normalized with respect to their maxima. The excitation spectrum was obtained using a deuterium light source from 120 to 300 nm combined with a xenon light source from 280 to 550 nm.

However, this only partly explains why we observe exclusively Sm^{2+} emission when exciting above 250 nm. There could be at least some weak Sm^{3+} emission due to the weak $4f \rightarrow 4f$ excitation of Sm^{3+}. This might be explained by assuming Sm^{3+} to be present as Sm_2O_3 nanoparticles. In such a scenario, the nearly 100% Sm^{3+} concentration in these particles is expected to largely quench its PL.

As discussed above, the optical and luminescence properties of reactive co-sputtered films only suggest a high Sm^{3+} content. A piece of more direct and clear evidence can be attested by XPS characterization of the film SLSm1. SLSm1 is a single-layer film with a gradient composition [16] that was prepared in a very similar way as reported in Ref. [5]. Fig. 3 gives the Sm $3d_{5/2}$ XPS edges in four different locations of SLSm1 after it was annealed at 574 °C for 15 min. Within Sm $3d_{5/2}$ peak, the divalent and trivalent states of Sm are resolved because of ($\approx$11 eV) difference in photoelectron binding energy. Table 4 gives the Sm^{2+}/Sm^{3+} ratio for each of the analyzed positions. In all probed points, Sm^{2+} was lower than 5.5 at% of the total Sm content.

3.2. MTFP for enhanced Sm^{2+} absorption

To overcome the poor absorption of Sm^{2+} caused by the high Sm^{3+} fraction in SiAlO:Sm, the MCR was taken as an inspiration to deposit multilayered thin-film precursors (MLSm1 and MLSm2) composed of SiAlO and metallic layers of Sm (SiAlO/m-Sm). Table 2 gives the details on the deposition conditions used for fabrication. To further test the viability of this procedure for reducing Ln ions in thin films, we also fabricated MTFP using Tm as the metallic lanthanide compound under similar conditions used for the MTFP based on Sm. The mere observation of Tm^{2+} luminescence in coatings prepared using this strategy is a strong indication that this method can produce materials with an enhanced fraction of Ln^{2+}.

To get more information on the general aspect of each individual layer of the MTFP, along with details of each layer's interface with the next, TEM imaging allied with EDX maps were made on a specifically
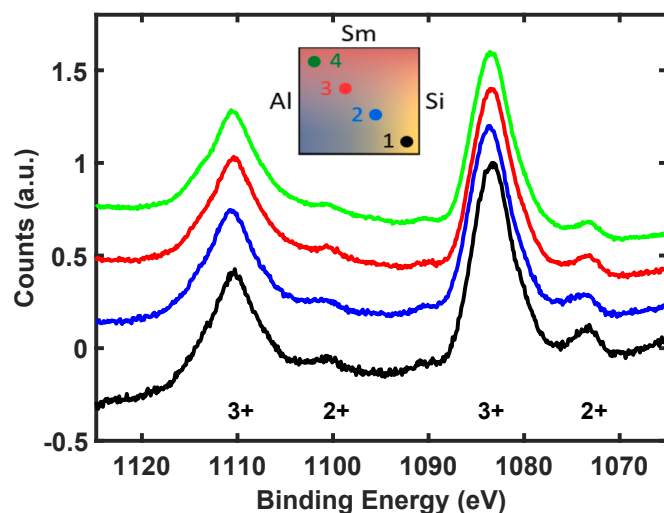
Fig. 3. Detailed XPS scans of Sm $3d_{3/2}$ (1110 eV) and $3d_{5/2}$ (1184 eV) edges measured at different positions on sample SLSm1. The spectra was obtained after annealing. All spectra are normalized to illustrate the ratio between Sm^{2+} and Sm^{3+}. The colored circles in the inset indicate at what position of the gradient sample the spectra with the corresponding color were measured. The spectra can be related to the data in Table 4 through the numbers 1–4 indicated in the inset.

Table 4
Atomic percentages of sample SLSm1 as derived from XPS survey spectra (details on the method are described in section 2.2). Measurements have been performed after annealing. Numbers 1–4 correspond to the positions at which the measurements have been performed on the gradient sample. The positions are indicated in the inset panel of Fig. 3 with colored dots corresponding to the colors of the spectra. Note that adventitious carbon was disregarded in the calculation, therefore the percentages of O, Si, Al and Sm together add up to 100%.

Pos.	O [at.%]	Si [at.%]	Al [at.%]	Sm [at.%]	Sm^{2+}/Sm [%]
1	64.0	34.7	0.7	0.5	5.5
2	65.0	33.3	1.0	0.7	4.5
3	64.0	33.5	1.5	1.0	4.4
4	64.5	32.1	2.0	1.4	3.3

designed MTFP made with metallic Tm layers (MLTm2). This multilayer film was prepared over c-Si substrate to ensure easy handling on the microscope. TEM images are shown in Fig. 4 for MLTm2 in as-deposited state. From TEM imaging, the total thickness of the film is 1225 nm, 7 SiAlO layers with $\approx$158 nm, and 7 metallic Tm layers $\approx$17 nm in thickness. The thicknesses of the metallic Sm and SiAlO layers were, however, systematically estimated by self-consistent fitting routines of the MTFP transmittance spectra in the UV-VIS spectral window. The routines used custom made models of the dielectric functions of metallic Sm and the SiAlO layers due to limitations on available information of the dielectric function specifically in the UV-VIS window. The fitting routine was run on RefFIT [20]. More details about the implementation of the method are in supplementary information.

Fig. 5 shows the normalized photoluminescence emission spectra of 5**A)** SLSm4 and 5**B)** MLSm2 when excited at 245 nm (blue) and 375 nm (red). Notice the large difference between the Sm^{3+} $4f \rightarrow 4f$ emission line intensity between SLSm4 and MLSm2, under resonant excitation through the Sm^{3+}'s charge transfer band. In MLSm2 no Sm^{3+}'s PL emission is observed which demonstrates a much lower Sm^{3+} content.

Fig. 6 shows the evolution of the transmittance of MLSm1 after annealing temperature and time in N_2/H_2 atmosphere. Before annealing, the films prepared by MTFP showed low transmittance, characteristic of metallic absorption from thin layers. The blue curve in Fig. 6**A)**
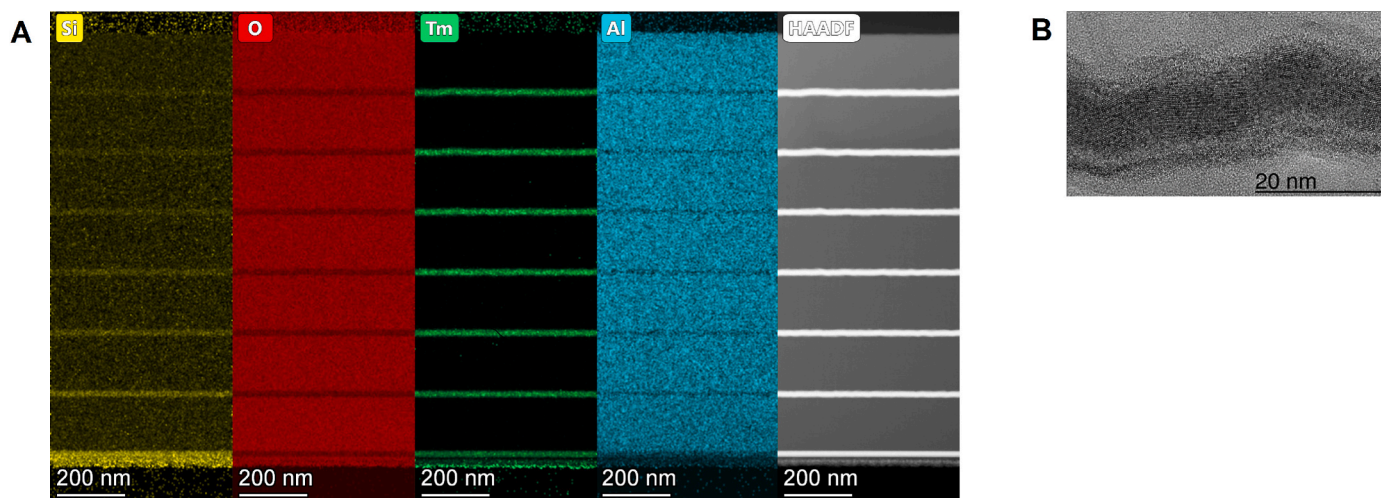
Fig. 4. TEM-EDX cross section maps of 7 layered SiAlO/m-Tm MTFP (sample MLTm2) in as-deposited state. **A)** From left to right: EDX maps of Si, O,Tm, Al, and ADF TEM image. **B)** Typical high resolution TEM image of one Tm layer grown by igniting only the Tm target in metallic mode. Notice layer irregularities and the presence of Tm-related nano-crystalline structures.
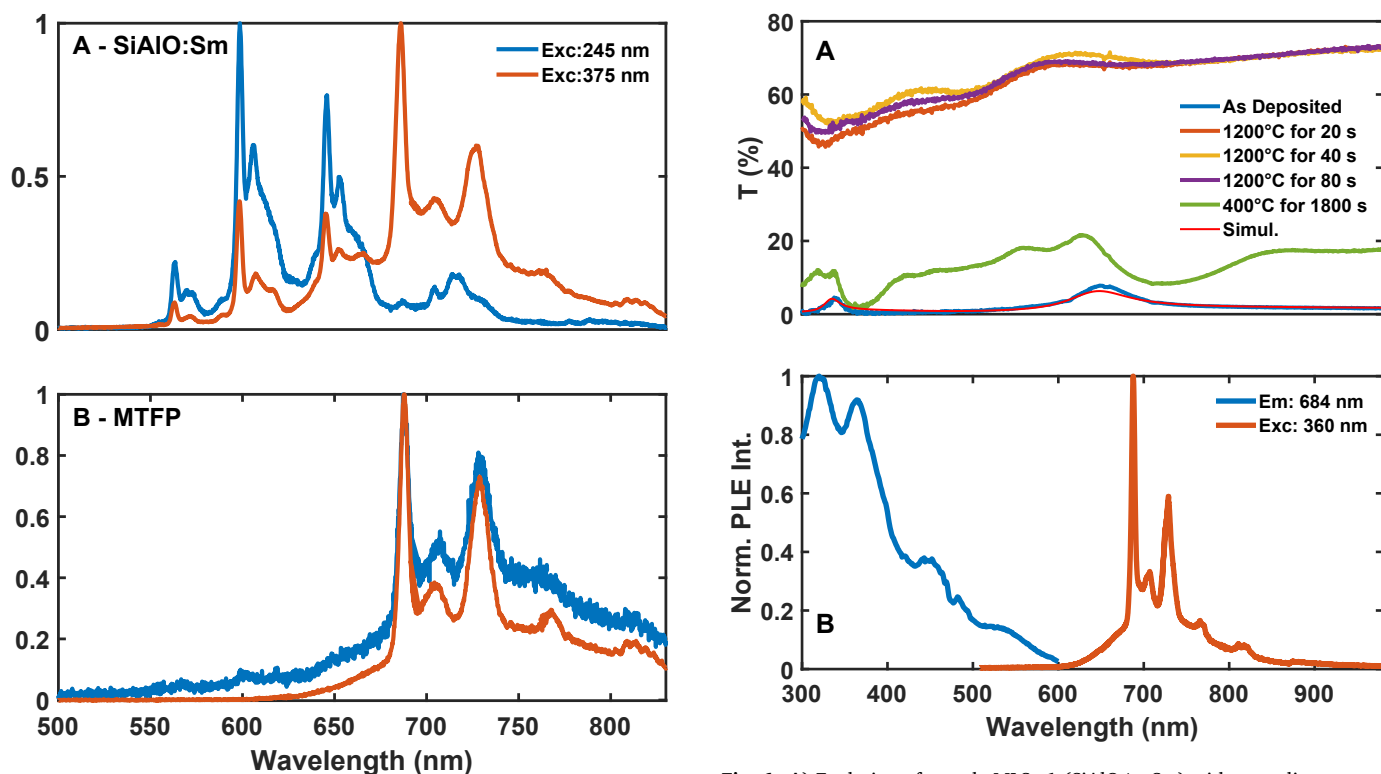

Fig. 5. Normalized photoluminescence emission spectra of **A)** SLSm4 and **B)** MLSm2 when excited at 245 nm (blue) and 375 nm (red).

Fig. 6. **A)** Evolution of sample MLSm1 (SiAlO/m-Sm) with annealing temperature and time. The sample becomes transparent with higher annealing temperature and slightly changes with longer annealing times at 1200 °C. In blue is MLSm1 in as-deposited state and, in red, is the transmittance simulated by RefFIT of 7 SiAlO 190 nm-thick layers interspersed with 7 metallic Sm 11 nm-thick layers. See supplementary information for more details on these simulations. **B)** Normalized excitation and emission photoluminescence spectra of sample MLSm1 after annealing treatment.

depicts the transmittance of MTFP before annealing. Overlayed to the transmittance spectrum of the as-deposited MTFP, in red, is the transmittance simulated by RefFIT. This simulation used 7 SiAlO layers with a thickness of 190 nm and seven metallic Sm layers (11 nm thick). More details on these values can be found in supplementary information. With progressive annealing of MTFP at increased temperatures, Sm is reduced while diffusing into the SiAlO layer. This oxidation reaction makes the coating progressively more transparent to a point where the transmittance reaches about 65–70% for wavelengths over 600 nm. Below 600 nm, however, the transmittance spectrum suggests the presence of two absorption bands (one between 350 and 370 nm and a second one
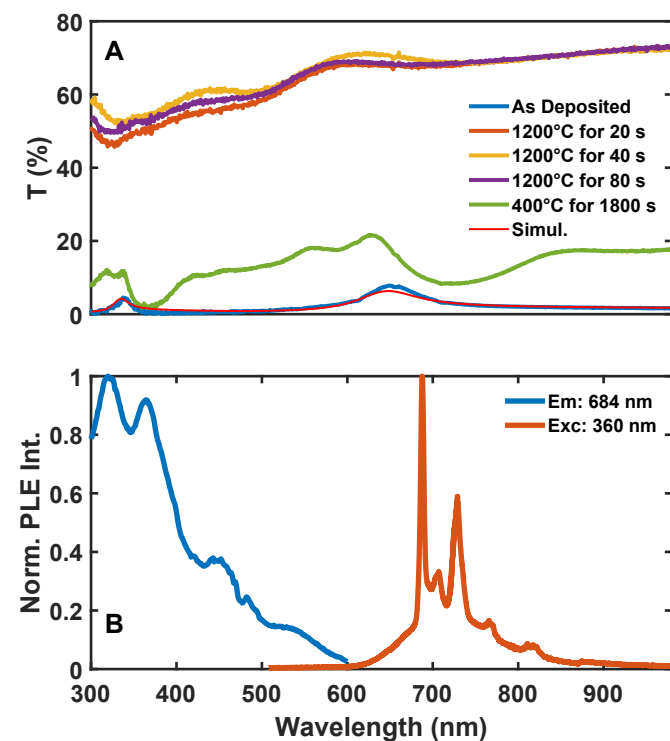
centered around 520 nm). The band matches with the main excitation band known for Sm^{2+} PL. The excitation of MLSm1, after all the annealing treatment, is shown in Fig. 6B).

A direct comparison between the co-sputtering and the MTFP strategies concerning obtaining enhanced Sm^{2+} absorption is given in Fig. 7. This figure shows the transmittance spectra of one Sm doped SiAlO
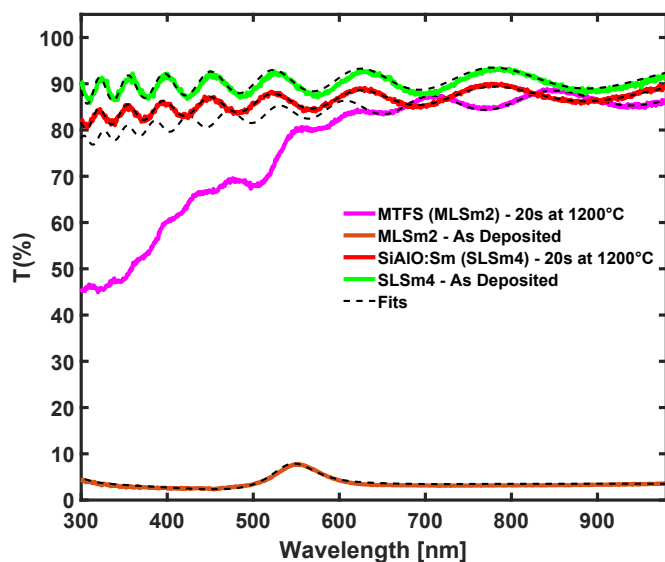
Fig. 7. Comparison of transmittance among one reactively co-sputtered SiAlO: Sm single-layered thin-film (SLSm4) and a MTFP (MLSm2), before and after rapid thermal annealing. See Table 2 for further details about the deposition conditions used for each sample.

prepared by MTFP (MLSm2) and reactive co-sputtering (SLSm4). SLSm4 was deposited with the same sputtering conditions used to grow the SiAlO layers in the MLSm2 except that the reactive sputtering of Sm target was done simultaneously to Al and Si targets.

We also present the effect of the same annealing treatment in both samples. The green curve represents SLSm4's transmittance in the as-deposited state, whereas the red curve gives the transmittance after annealing. The orange curve represents the transmittance spectra of MLSm2 before annealing, and the pink, its transmittance after annealing. The typical interference fringe structure of SLSm4 is characteristic of a homogeneous thin film layer with a different refractive index than the substrate and the amplitude of the fringes is a consequence of the difference in refractive index, and the number of fringes usually corresponds to the film thickness (the more fringes, the thicker the film).

The transmittance spectra of SLSm4 are fitted with a refractive index's dispersion relation of the Sellmeier type. The extinction coefficient dispersion was modeled assuming an absorption bandgap zone with a Taylor expansion [25]. The most relevant effects of the annealing on this sample are a slight decrease of the transmittance across the UV-VIS spectrum accompanied by an increase in its thickness. The dashed lines on the green, red, and pink curves represent the results of a fitting routine of thin films using OPTIFIT [17]. The dashed line on the orange transmittance curve is a fit made from the method described in supplementary information. We credit the change in thickness to a possible plastic deformation caused by thermal expansion. Due to the possible formation of nanocrystals, the presence of grain boundaries can increase scattering, thus lowering the transmittance across the visible spectrum. For what is worth, absorption by Sm^{2+} can not be clearly observed in SLSm4.

A more striking change is evident in the transmittance of MLSm2. Because of the cost and time needed to prepare samples for TEM characterization, we used another method to estimate individual layer thickness by more easily accessible optical transmission measurements (see supplementary information for more details). Table 5 summarizes the refractive index and thickness of the layers considered here. Before the annealing treatment, MLSm2 is, by visual inspection, an opaque film with a shiny reflectance typical of metallic materials. It can be well modeled by eight 188 nm-thick SiAlO layers alternated by eight metallic Sm layers of 11 nm in thickness. After annealing at 400 °C for 30 min followed by 1200 °C during 20 s in N_2/H_2 gas, the transmittance

Table 5

Thicknesses retrieved by UV-VIS transmittance fitting shown in Figs. 6 and 7. The refractive indices reported are retrieved at 585 nm.

Sample ID	Annealing Condition	Total	SiAlO		RE	
		d [nm]	d [nm]	n	d [nm]	n
SLSm4	As Deposited	968	968	1.61	N/A	
SLSm4	Annealed at 1200 °C	982	982	1.59	N/A	
MLSm1	As Deposited	1456	199	1.54	10	2.23
MLSm2	As Deposited	1344	160	1.54	8	2.23
MLTm1	As Deposited	1582	220	1.54	6	2.23

spectrum has two distinct regions. In wavelengths longer than 600 nm, it shows the typical interference fringes structure of a transparent film. This can be well described by a model of a transparent film ($\kappa \approx 0$). The amplitude is the same as the observed for sample SLSm4, i.e., MLSm2 has a similar refractive index as SLSm4. For wavelengths below 600 nm, however, the transmittance is characterized by higher absorption (lower transmittance). The minimum transmittance is situated between 320 and 370 nm. As shown by Fig. 6**B**, this corresponds well with the highest excitation band of Sm^{2+}.

In Fig. 8 a comparison between the photoluminescence emission intensity of samples SLSm6 (blue), MLSm2 (red), and SLSm4 (yellow) is shown when excited using the same excitation conditions, i.e., 375 nm excitation wavelength from a ThorLabs LED. These samples had their photoluminescence quantum efficiency (PLQE) characterized in a separate experiment described in supplementary information. Among these samples, SLSm6 has the highest PLQE despite not showing any noticeable Sm^{2+}-related absorption (as shown in Fig. 7). Sample MLSm2 has a strong Sm^{2+}-related absorption (shown in Fig. 7) and a low PLQE ($\approx 0.20\%$). As a comparison measure, the integrated emission intensity of MLSm2, being a product of quantum efficiency and absorption, is about 60% of the sample with the best quantum efficiency (SLSm6). These results indicate that the strategy using MTFP is still worthy of further investigation when considering LSC applications.

MLSm2 and SLSm4 were prepared so that the composition of the SiAlO layers are comparable after annealing treatment was performed. In terms of sputtering deposition, SLSm4 was grown with the same conditions as the SiAlO layers of MLSm2 (see Table 2). The only exception being the Sm target that was also operated at 30 W with both Si and Al targets fully oxidized. As it is shown by Table 6 both SLSm4 and MLSm2 have very similar SiAlO composition (despite MLSm2 shows
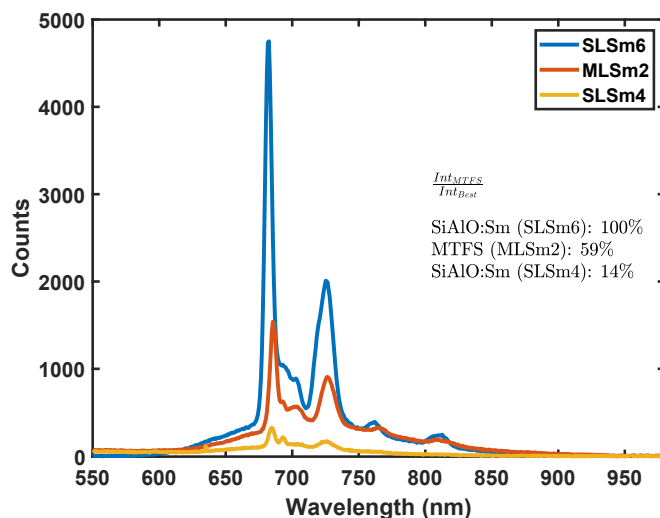

Fig. 8. Comparison of the photoluminescence emission intensity between samples SLSm6 (blue), MLSm2 (red), and SLSm4 (yellow) excited at 375 nm. The numbers in the inset compare the total integrated intensity (between 550 and 950 nm) of each sample with the PL intensity observed in SLSm6.

Table 6
Composition, quantum efficiency (Q.E.), and absorption (Abs.) at 375 nm of samples MLSm2 and SLSm4 (after annealing treatment) obtained by SEM/EDS operated at 15 keV. Quantitative elemental analysis without a conductive coating was achieved by employing the device in low vacuum mode (35 Pa pressure). Elemental compositions were quantified at $100 \times$ magnification. Further details about the methods used to determine Q.E. are in supplementary information.

Sample ID	O [at. %]	Si [at. %]	Al [at. %]	Sm [at.%]	Energy [kV]	Q.E. [%]	Abs. [%]
SLSm4	61.4	5.4	32.9	1.2	15	0.13	11.2
MLSm2	60.9	5.2	31.6	2.3	15	0.20	57.4
SLSm6	65.6	32.0	2.0	0.4	15	13.0	6.0

twice as much Sm). The comparison of the photoluminescence between MLSm2 and SLSm4 in Fig. 8 shows that, while the quantum efficiency of SLSm4 is higher than the one of MLSm2, SLSm4's poor Sm^{2+}-related absorption is so low that the total integrated emission observed in SLSm2 is lower than the one observed in MLSm2.

3.3. Divalent thulium in Tm doped SiAlO prepared by MTFP

As notoriously known, Tm^{2+} is much less stable than Sm^{2+}. In oxides, Tm^{2+} is rather anomalous. Except from SrB_4O_7, Tm^{2+} was only previously stabilized on di-halide or halidoperovskite crystals [9,26,27]. Being known for having a wide absorption over the visible range and possessing a very low self-absorption, Tm^{2+} has been recently considered for LSC applications [28,29]. Its properties are characterized by strong absorption from the UV up to 900 nm due to $4f^{13} \rightarrow 4f^{12}5d^1$ electronic transitions and a single and narrow luminescence emission line in near-infrared (NIR) - credited to the $^2F_{5/2} \rightarrow {}^2F_{7/2}$ transition. Tm^{2+} doped CaI_2 showed 65% absorption of the solar spectral range while showing no self-absorption and a relatively neutral color [27]. However, halide hygroscopicity prevents these coatings from direct upscaling using glass-industry standards.

Here we show that the MTFP strategy can be used to produce SiAlO: Tm with Tm^{2+} when the SiAlO host is in the mullite region. Fig. 9 shows normalized excitation and emission photoluminescence spectra out of Tm^{2+} in sample MLTm1 (dark blue), prepared through MTFP strategy. SSRTm (light blue), prepared through sol-gel synthesis (phosphor), is also shown for comparison. More details on how SSRTm was prepared
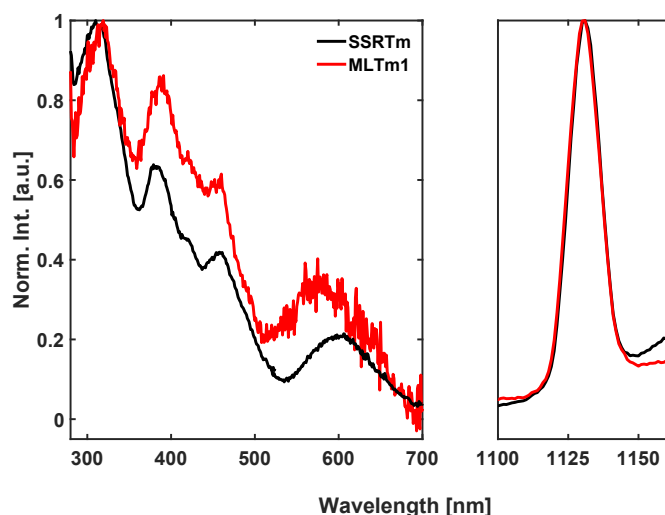
can be found in Table 3.

Before being able to exhibit $^2F_{5/2} \rightarrow {}^2F_{7/2}$ transitions of Tm^{2+}, MLTm1 had to be rapid thermally annealed (one 30-min step at 400 °C, followed by another at 1200 °C for 20 s). Both samples have their excitation spectra obtained by monitoring the emission intensity at 1132 nm. The emission spectra were obtained after laser excitation near 470 nm. An excitation wavelength of 465 nm was used for the MTFP, whereas the emission spectrum of SSRTm was recorded after excitation at 470 nm. Further details on these measurements can be found in section 2.3. Similar films prepared using a more conventional reactive co-sputtering of Si, Al, and Tm targets did not show any Tm^{2+} photoluminescence. The observation of Tm^{2+} doped SiAlO thin-films using the MTFP strategy brings alternative routes with potential towards the creation of new divalent-lanthanide-based LSC materials that are compatible with the installed glass-industry infrastructure.

Any possible application employing the MTFP strategy for LSC applications requires reducing the high temperatures necessary to diffuse metallic Tm. Additionally, a deeper understanding is needed of the causes for the low quantum efficiency observed in MTFP using Sm, and possibly also Tm. With this knowledge, alternative processes can be chosen to lower annealing temperatures and increase quantum efficiencies.

One possible cause of the low efficiency can be the low solubility of the trivalent Ln elements in materials of the SiAlON class. Due to larger ionic radii, the solubility of divalent lanthanide elements is even lower. Thus, there is a good possibility of agglomerates of Ln ions or the presence of phase segregation that can potentially be responsible for the observed low quantum efficiency when compared to the straightforward co-sputtering method. Preliminary STEM diffraction studies on the annealed films prepared using MTFP revealed many possible crystalline structures. To precisely pinpoint the crystal phases correlated with Tm^{2+} luminescence, another study, combining STEM and cathodoluminescence, would be greatly beneficial.

4. Conclusion

XPS characterization of the Sm $3d_{5/2}$ edge of reactive magnetron co-sputtered Sm doped SiAlO thin-films with gradient composition has revealed a low concentration of Sm^{2+} (in the ratio of 3–5 at.% to the total amount of Sm). This explains the weak absorption in the 300–600 nm wavelength range of thick and heavily Sm doped films. The weak Sm^{3+} $4f \rightarrow 4f$, when compared to the Sm^{2+} $4f \rightarrow 5d$ absorption cross-section, explains that we still observe mainly Sm^{2+} emission when excited in this range.

Inspired by the comproportionation reaction from solid-state synthesis, the MTFP strategy results in the formation of the divalent state of Sm and Tm. SiAlO:Sm materials with enhanced Sm^{2+} absorption are observed when compared to single-layered films prepared by reactive magnetron co-sputtered materials with similar composition. The advantage of this thin-film deposition procedure is its potential compatibility with glass industry standards. We reckon that full scalability requires much lower annealing temperatures (typically below 650 °C). Using the same strategy, we have also shown that it becomes possible to obtain the exotic Tm^{2+} doped in SiAlO related thin films by observing the characteristic Tm^{2+} NIR photoluminescence peak at 1132 nm.

To access further the potential of the MTFP strategy based on the optical properties of Sm^{2+} and Tm^{2+}, more research with other industry-compatible hosts having higher solubility to Sm^{2+} and Tm^{2+} (or higher Ln diffusivity coefficient) would be beneficial. One more relevant research direction would explore the combined effect of doping each SiAlO layer with Sm^{2+} (or Tm^{2+} in the case of SiAlO:Tm) and employing the metallic layer precursors.

Fig. 9. (Left) Normalized photoluminescence excitation spectra of SSRTm (black) and MLTm1 (red) obtained by monitoring the emission at 1130 nm. (Right) Normalized photoluminescence emission spectra of the same samples in black and red (excitation at 470 nm). Further data acquisition details are in section 2.3.

Author statement

G.B.F. Bosco: Conceptualization, Supervision, Project administration, Writing – original draft preparation, Writing – review & editing, Data curation, Visualization. J.K. van den Biesen: Investigation, Data curation, Writing – original draft preparation. C.D. Boers: Investigation. G. Simone: Investigation. J. Kao: Investigation. F.D. Tichelaar: Investigation, and Formal Analysis. B. Boshuizen: Investigation. E. van der Kolk: Funding acquisition, Resources, Supervision, Writing - review.

Declaration of competing interest

The authors declare that they have no known competing financial interests or personal relationships that could have appeared to influence the work reported in this paper.

Appendix A. Supplementary data

Supplementary data to this article can be found online at https://doi.org/10.1016/j.jlumin.2021.118421. The dataset and scripts used for generating the plots in this work are available at https://doi.org/10.4121/14798358.v1.

References

[1] C.J. Traverse, R. Pandey, M.C. Barr, R.R. Lunt, Emergence of highly transparent photovoltaics for distributed applications, Nat. Energy 2 (2017) 849–860.

[2] O.M. ten Kate, K.M. Hooning, E. van der Kolk, Quantifying self-absorption losses in luminescent solar concentrators, Appl. Opt. 53 (2014) 5238.

[3] E.P. Merkx, S. van Overbeek, E. van der Kolk, Functionalizing window coatings with luminescence centers by combinatorial sputtering of scatter-free amorphous SiAlON:Eu2+ thin film composition libraries, J. Lumin. 208 (2019) 51–56.

[4] D. K. de Boer, C. R. Ronda, W. Keur, A. Meijerink, New luminescent materials and filters for luminescent solar concentrators, in: High and Low Concentrator Systems for Solar Electric Applications VI, volume 8108, International Society for Optics and Photonics, p. 81080E.

[5] D. de Vries, S. van Overbeek, E.P. Merkx, E. van der Kolk, Sm2+-doped SiAlO sputter deposited coatings for self-absorption and scatter-free luminescent solar concentrator applications, J. Lumin. 225 (2020) 117321.

[6] E.P. Merkx, S. van Overbeek, E. van der Kolk, Functionalizing window coatings with luminescence centers by combinatorial sputtering of scatter-free amorphous SiAlON:Eu2+ thin film composition libraries, J. Lumin. 208 (2019) 51–56.

[7] S. Stojadinović, N. Tadić, R. Vasilić, Photoluminescence of Sm2+/Sm3+ doped Al2O3 coatings formed by plasma electrolytic oxidation of aluminum, J. Lumin. 192 (2017) 110–116.

[8] P. Dorenbos, Charge transfer bands in optical materials and related defect level location, Opt. Mater. 69 (2017) 8–22.

[9] M. Suta, C. Wickleder, Synthesis, spectroscopic properties and applications of divalent lanthanides apart from Eu 2+, J. Lumin. 210 (2019) 210–238.

[10] G. Meyer, The divalent state in solid rare earth metal halides, Rare-earth Elem. (2012) 1–13.

[11] J. Grimm, E. Beurer, H.U. Güdel, Crystal absorption spectra in the region of 4f- 4f and 4f- 5d excitations in tm2+-doped cscacl3, cscabr3, and cscai3, Inorg. Chem. 45 (2006) 10905–10908.

[12] O.S. Wenger, C. Wickleder, K.W. Krämer, H.U. Güdel, Upconversion in a divalent rare earth ion: optical absorption and luminescence spectroscopy of tm^{2+} doped srcl$_2$, J. Lumin. 94 (2001) 101–105.

[13] C.-G. Ma, M. Brik, D.-X. Liu, B. Feng, Y. Tian, A. Suchocki, Energy level schemes of fn electronic configurations for the di-, tri-, and tetravalent lanthanides and actinides in a free state, J. Lumin. 170 (2016) 369–374 (SI: Lanthanide spectroscopy).

[14] V. Alexander, Anna Kraut-Vass Naumkin, Stephen W. Gaarenstroom, Cedric J. Powell, NIST X-Ray Photoelectron Spectroscopy Database, 2012.

[15] N. Fairley, CasaXPS Manual: Introduction to XPS and AES, 2009.

[16] E.P. Merkx, E. Van Der Kolk, Method for the detailed characterization of cosputtered inorganic luminescent material libraries, ACS Comb. Sci. 20 (2018) 595–601.

[17] R. Alvarez, A. Garcia-Valenzuela, C. Lopez-Santos, F.J. Ferrer, V. Rico, E. Guillen, M. Alcon-Camas, R. Escobar-Galindo, A.R. Gonzalez-Elipe, A. Palmero, High-rate deposition of stoichiometric compounds by reactive magnetron sputtering at Oblique Angles, Plasma Process. Polym. 13 (2016) 960–964.

[18] R. Swanepoel, Determination of the thickness and optical constants of amorphous Ge-Se-Bi thin films, Phil. Mag. 89 (1983) 1005–1016.

[19] D. Poelman, P.F. Smet, Methods for the determination of the optical constants of thin films from single transmission measurements: a critical review, J. Phys. Appl. Phys. 36 (2003) 1850–1857.

[20] A.B. Kuzmenko, Kramers–Kronig constrained variational analysis of optical spectra, Rev. Sci. Instrum. 76 (2005) 83108.

[21] Y. Yoshino, K. Inoue, M. Takeuchi, K. Ohwada, Effects of interface micro structure in crystallization of ZnO thin films prepared by radio frequency sputtering, Vacuum 51 (1998) 601–607.

[22] D. Smith, Deposition, in: Thin-Film Deposition: Principles and Practice, internatio edition, McGraw-Hill, Singapore, 1997, pp. 180–185.

[23] G. Zhu, J. Sun, L. Zhang, Z. Gan, Molecular dynamics simulation of temperature effects on deposition of Cu film on Si by magnetron sputtering, J. Cryst. Growth 492 (2018) 60–66.

[24] Z. Xia, D. Chen, Synthesis and luminescence properties of bamoo4: Sm3+ phosphors, J. Am. Ceram. Soc. 93 (2010) 1397–1401.

[25] R. Alvarez, A. Garcia-Valenzuela, C. Lopez-Santos, F.J. Ferrer, V. Rico, E. Guillen, M. Alcon-Camas, R. Escobar-Galindo, A.R. Gonzalez-Elipe, A. Palmero, High-rate deposition of stoichiometric compounds by reactive magnetron sputtering at Oblique Angles, Plasma Process. Polym. 13 (2016) 960–964.

[26] P. Solarz, J. Komar, M. Głowacki, M. Berkowski, W. Ryba-Romanowski, Spectroscopic characterization of SrB 4 O 7 :Tm 2+ , a potential laser material and optical temperature sensor, RSC Adv. 7 (2017) 21085–21092.

[27] O.M. Ten Kate, K.W. Krämer, E. Van Der Kolk, Efficient luminescent solar concentrators based on self-absorption free, Tm2+ doped halides, Sol. Energy Mater. Sol. Cell. 140 (2015) 115–120.

[28] M. De Jong, W. Kesteloo, E. Van Der Kolk, Deposition of luminescent NaCl:Tm2+ thin films with a Tm concentration gradient using RF magnetron sputtering, Opt. Mater. 46 (2015) 149–153.

[29] E.P.J. Merkx, E. Van Der Kolk, Luminescent solar concentrators, in: Indoor Photovoltaics: Materials, Modeling and Applications, Wiley Online Library, Delft, 2020, pp. 133–188.